2013 IEEE International Conference on Robotics and Automation (ICRA)
Karlsruhe, Germany, May 6-10, 2013

Muscle-Reflex Control of Robust Swing Leg Placement

Ruta Desai and Hartmut Geyer

Abstract— **Swing leg placement is vital to dynamic stability in legged robots and animals. The most common approaches to generating swing leg motions in robotics use either position or impedance tracking of defined joint trajectories. While these approaches suffice in humanoids, they severely limit swing leg placement under large disturbances in prosthetic limbs, for which stabilizing reactions cannot be planned centrally. We previously identified a control for a conceptual double-pendulum swing leg that does not require predefined trajectories to robustly place the leg into target points on the ground in the presence of large disturbances. We here develop a more detailed neuromuscular model of the human swing leg and interpret the identified control with local muscle reflexes. The resulting reflex control robustly places the swing leg into a wide range of landing points observed in human walking and running, and it generates similar patterns of joint torques and muscle activations. While we plan to take advantage of the comparison between the neuromuscular model and humans to further improve robust swing leg placement, the current results suggest an alternative to existing swing leg controls in humanoid and rehabilitation robotics which does not require central processing.**

I. Introduction

Swing leg placement is vital to stability in legged robots and animals. Without placing the feet into proper target points on the ground, legged systems fail to balance dynamically [1]. These placement targets have been identified for walking and running with point-mass models, which can stabilize gait in response to a disturbance such as an external push or an unexpected change in the ground level [2]–[6]. However, these conceptual models do not reveal how the segmented legs of humans and humanoids actually get to these targets.

The common approach to generating swing leg motions in humanoids relies on trajectory planning and tracking. Trajectories for all the leg joints are planned either based on cost optimization [7] or by interpolation between consecutive placement targets [8], [9]. Once generated, these reference trajectories are tracked via proportional-derivative control at each joint. This approach to swing leg motions requires central control over all leg joints, making it difficult to use in prosthetic limbs which replace only part of the human body.

Although alternative approaches have been explored in rehabilitation robotics [10], tracking predefined joint patterns remains the state of the art in the control of powered prosthetic legs [11]–[13]. In effect, prosthetic legs show only limited dexterity in recovering gait after disturbances.

This work is supported in part by the NSF through the NSF ERC on Quality of Life Technology (EEC 0540865) and by NIH through the NICHD National Center for Medical Rehabilitation Research (1R01HD075492-01). R. Desai and H. Geyer are with the Robotics Institute, Carnegie Mellon University, 5000 Forbes Avenue, Pittsburgh, PA 15213, USA. {rutad,hgeyer}@cmu.edu

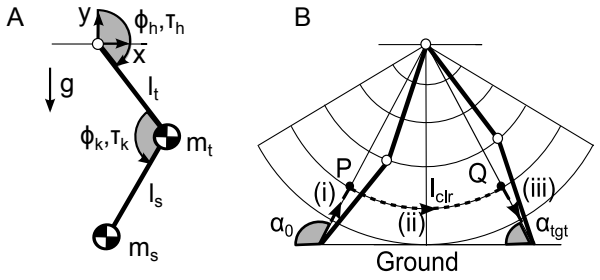

Fig. 1. Idealized model and control for robust swing leg placement (**A**) Conceptual double pendulum model of leg swing with point masses at the ends of massless segments of equal length l_s. (**B**) Sequence of natural control tasks for reaching a target leg angle α_{tgt} from an initial angle α_0 while guaranteeing foot ground clearance l_{clr}.

Animal and human legs by contrast demonstrate robust swing placement with remarkable autonomy. From early work on mesencephalic cats [14] to recent investigations on paralyzed cats and rats with drug administration and epidural stimulation [15], experiments have shown that animals can seamlessly adapt their leg behavior in stance and swing to different speeds and gaits without central planning by the brain. These observations suggest that a substantial part of leg control in animal and human gait is generated by spinal circuits which adapt to changes in the environment [16].

Inspired by these observations, we previously developed a control for a double pendulum leg in swing that is based on local feedbacks and does not require predefined trajectories to robustly place the leg into target points on the ground in the presence of large disturbances [17]. However, we neither modeled the foot segment of human and humanoid legs, nor considered the neuromuscular system with its actuation and control limitations. To compare the identified control with human swing leg behavior at the level of muscle activations, and to prepare a transfer to powered prosthetic legs that react like human limbs, we here develop a neuromuscular model of the human leg in swing and interpret the identified control with local muscle reflexes. We first summarize the previously identified control (Sec. II), then interpret it with the neuromuscular model (Sec. III), and finally compare and discuss the resulting leg placement performance with respect to the previous control and to human data on swing leg motions in walking and running (Sec. IV and V).

II. Modular Swing-Leg Placement Control

The previously identified control [17] is based on the double pendulum analogy of the human swing leg (Fig. 1A) and takes advantage of the natural pendulum dynamics to achieve robust swing leg placement without enforcing predefined

reference trajectories of the foot. The control uses a target leg angle α_{tgt} and a clearance leg length l_{clr} as inputs, and it implements a natural sequence of three control tasks which comprise flexing the leg to the clearance length, advancing the leg to the target angle, and extending the leg until ground contact (Fig. 1B). In addition to taking advantage of passive dynamics for energy efficiency, the control is separated between the hip and knee as much as possible to enable modular implementation in artificial legs that replace only part of human limbs.

The hip portion of the control is realized as a proportional-derivative control

$$\tau_h = k_p^{\alpha}(\alpha_{tgt} - \alpha) - k_d^{\alpha}\dot{\alpha} + \tau_h^{iii}, \tag{1}$$

where τ_h is the commanded hip torque, α and $\dot{\alpha}$ are the current leg angle and angular velocity, and k_p^{α} and k_d^{α} are proportional and derivative gains. Note that a positive input tends to extend the hip (Fig. 1A). The additional torque component τ_h^{iii} results from biarticular actuation that is commanded by the knee control during the last, leg extension task of the control sequence. It is the only interaction control between the two joints.

The knee portion is divided into three parts which follow the natural control sequence. In the first part, the knee actively flexes in proportion to how fast the leg moves forward,

$$\tau_k^i = \begin{cases} k^i\dot{\alpha}, & \dot{\alpha} \le 0 \\ 0, & \dot{\alpha} > 0 \end{cases}, \tag{2}$$

where τ_k^i is the resulting knee torque and k^i is a proportional gain. Once the leg shortens past the clearance length, $l < l_{clr}$, the second part of the knee control engages with

$$\tau_k^{ii} = \begin{cases} -k^{ii}\dot{\phi}_k, & \dot{\phi}_k \le 0 \\ -k^{ii}\dot{\phi}_k(\alpha - \alpha_{tgt})(\dot{\phi}_k + \dot{\alpha}), & \dot{\phi}_k > 0 \;\&\; \dot{\phi}_k > -\dot{\alpha} \\ 0, & \text{otherwise} \end{cases}. \tag{3}$$

This part realizes holding the knee with a damping input (gain k^{ii}) that is pure when the knee flexes ($\dot{\phi}_k \le 0$) and modulated when it extends ($\dot{\phi}_k > 0$). The modulation allows passive extension to take effect when α approaches its target ($\alpha - \alpha_{tgt}$), but prevents premature landing if the knee extends faster than the leg moves toward the target during the approach ($\dot{\phi}_k + \dot{\alpha}$). The final part of the knee control engages when the leg angle passes a threshold $\alpha_{thr} = \alpha_{tgt} + \Delta\alpha_{thr}$. It realizes a stopping torque

$$\tau_k^{iii} = \begin{cases} -k^{stp}\left(\alpha_{thr} - \alpha\right)\left(1 - \frac{\dot{\alpha}}{\dot{\alpha}_{max}}\right), & \alpha < \alpha_{thr} \\ & \dot{\alpha} < \dot{\alpha}_{max} \\ 0, & \text{otherwise} \end{cases} \tag{4}$$

that is inspired by nonlinear contact models [18], [19], where k^{stp} is a proportional gain and $\dot{\alpha}_{max}$ describes a maximum return velocity. To cancel the effect of this stopping torque on the hip motion, it is compensated for by the hip torque component $\tau_h^{iii} = -2\tau_k^{iii}$ (Eq. 1). Further, an extension torque

$$\tau_k^{iii'} = \tau_k^{iii} + k^{ext}(l_0 - l), \tag{5}$$

is added once the leg angular has slowed down ($\dot{\alpha} = 0$),where k^{ext} is a proportional gain and $l_0 = 2l_s$.

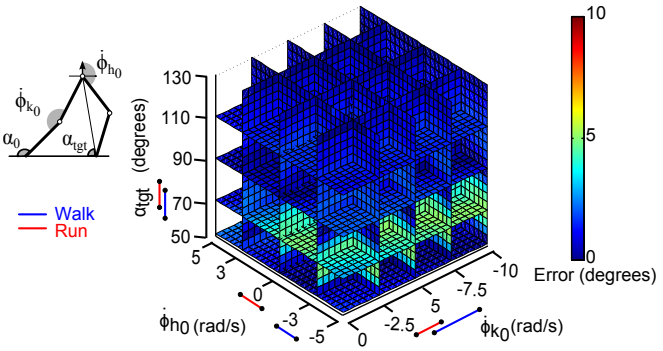

Fig. 2. Swing leg placement into arbitrary targets under large variation in initial conditions. The error $\Delta\alpha = \alpha_{tgt} - \alpha_l$ between the target angle and the achieved landing angle is shown as a color code for a large range of initial hip and knee velocities that cover the initial joint velocities observed in human locomotion from 0.65ms^{-1} to 5.5ms^{-1}.

Fig. 2 shows the performance that the control achieves for largely different initial swing velocities exceeding the range of joint velocities observed in human walking and running. Despite these large differences, the leg gets placed into target angles ranging from 50 deg to 130 deg with average and maximum placement errors of 1.4 deg and 5.2 deg, respectively. In addition, when applied to a more realistic model of human swing leg motion that includes hip translational accelerations and anthropometric segment mass distributions, the control generates swing leg motions and joint torque patterns that match human data well (not shown). However, the performance is based on an idealized model which does neither include the human foot nor represent the human neuromuscular system.

III. Neuromuscular Control Interpretation

To compare the identified control with human swing leg behavior at the level of muscle activations, and to prepare a transfer to artificial powered legs that can react like human limbs, we develop a neuromuscular model of the human leg in swing and interpret the modular control with local muscle reflexes. The model comprises three segments connected by revolute joints. The segments have anthropomorphic mass and inertia properties [20] and the joints represent hip, knee and ankle. Nine Hill-type muscle models span these joints, each consisting of a contractile element CE, and parallel and series elasticities (Fig. 3). A muscle produces the net force

$$F^m = F^m_{max} f_l f_v A^m$$

that is dependent on its maximum isometric force F^m_{max}, the force-length (f_l) and force-velocity relationships (f_v) of the contractile element, and the muscle activation A^m (see [19] for details on the muscle models). The muscle force translates into the joint torque contribution $\tau_j^m =$

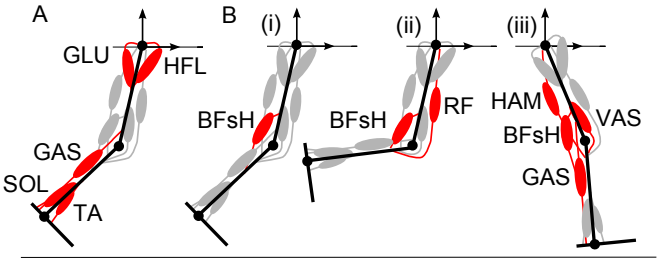

Fig. 3. Neuromuscular model for swing leg placement. (**A**) The ankle is controlled by the soleus (SOL), gastrocnemius (GAS), and tibialis anterior (TA) muscles as in [19]. The hip is flexed and extended by monoarticular hip flexor (HFL) and glutei (GLU) muscle groups. (**B**) The knee control is divided into the three tasks of the previously identified control. (i) Initial flexion is generated by the monoarticular biceps femoris short head muscle (BFsH). (ii) The knee is constrained by rectus femoris (RF) during hyper-flexion and by BFsH during extension. (iii) The hamstring muscle group (HAM) and the vastii group (VAS) brake and extend the leg. In addition, HAM recruits GAS and BFsH to prevent knee hyper-extension.

$F^m r_j^m$ at the joints j the muscle spans, where r_j^m is the muscle moment arm. The activation is related to the neural stimulation $S_m \in [0,1]$ of a muscle by

$$\dot{A}^m = (S^m - A^m)/\tau_{ecc},$$

where the constant $\tau_{ecc} = 10$ms describes the excitation-contraction coupling of muscle tissue [19].

For the muscle reflex interpretation of the modular leg placement control described in section II, the muscle stimulations are generated by local proprioceptive feedbacks from the same or other muscles (general index n),

$$S^m(t) = S_0^m + \sum_n G_n^m P_n^m(t - \Delta t_n^m), \tag{6}$$

where S_0^m is the muscle prestimulation, G_n^m is a feedback gain, P_n^m is the proprioceptive signal, Δt_n^m represents the neural transport delay [19], and the sum symbol describes α-motoneurons which can combine multiple feedbacks to generate the muscle net stimulation. The proprioceptive signals P_n^m are either length or velocity signals from the originating muscle n with

$$L_n^m = l_{ce}^n - l_{off}^n \text{ and } V_n^m = v_{ce}^n - v_{off}^n, \tag{7}$$

respectively. The offset values l_{off}^n and v_{off}^n model set point adjustments that γ-motoneurons can generate at muscle spindles, the sensory organs which measure muscle length and velocity [21]. Note that the muscle stimulation (6) is saturated between zero and one, reflecting that neurons modulate signals with firing rates that cannot become negative.

A. Leg Angle Estimation with Biarticular Muscle Stretch

The control described in section II requires the leg angle as a main input. This quantity can be estimated in the human neuromuscular system by the length of two biarticular muscles, the hamstring (HAM) and the rectus femoris (RF). Both muscles span the hip and knee. HAM is a hip extensor and knee flexor while RF flexes the hip and extends the knee. The lengths of the two muscles are given by

$$l^m = l_0^m \pm r_h^m(\phi_h - \phi_{h,r}^m) \mp r_k^m(\phi_k - \phi_{k,r}^m) \tag{8}$$

where l_0^m is the muscle rest length that is reached at the leg configuration defined by $\phi_{h,r}^m$ and $\phi_{k,r}^m$, and r_h^m and r_k^m are muscle moment arms at the hip and knee, respectively (top/bottom version for RF/HAM). In humans, $r_k^m \approx r_h^m/2$ for RF and HAM, and the leg angle relates to the hip and knee angles by $\alpha \approx \phi_h - \phi_k/2$ [17]. Equation 8 thus simplifies to

$$l^m = l_0^m \pm r_h^m(\alpha - \alpha_r^m)$$

with $\alpha_r^m = \phi_{h,r}^m - \phi_{k,r}^m/2$. On the other hand, in muscle $l^m = l_{ce}^m + l_{se}^m$. Assuming that the series elasticity does not stretch substantially beyond its slack length (l_{sl}^m) in these muscles, $l_{se}^m = l_{sl}^m$ (due to the low forces required in swing), the leg angle resolves to $\alpha = \pm(l_{ce}^m + l_{sl}^m - l_0^m)/r_h^m + \alpha_r^m$. Now, the control described in section II requires leg angle inputs only as differences $\alpha - \alpha_i$ with respect to target values α_i, which resolves to

$$\alpha - \alpha_i = \pm 1/r_h^m \ (l_{ce}^m - l_{off}^m) \tag{9}$$

when choosing the offset $l_{off}^m = \pm r_h^m(\alpha_i - \alpha_r^m) - l_{sl}^m + l_0^m$. Equation (9) describes a muscle spindle length feedback (6,7) of either the RF or the HAM. Likewise, the leg angular velocity can be estimated by the spindle velocity feedback of these biarticular muscles,

$$\dot{\alpha} = \pm 1/r_h^m \ (v_{ce}^m - v_{off}^m) \text{ with } v_{off}^m = 0. \tag{10}$$

B. Ankle Control

For the control of the added ankle, we use the same muscles and reflexes as in [19]. Three muscles actuate the ankle, the monoarticular soleus (SOL) and tibialis anterior (TA) muscles as well as the biarticular gastrocnemius muscle (GAS) (Fig. 3A). While the ankle extensors SOL and GAS do not actively contribute to ankle control in swing, TA gets stimulated by its own length feedback $S^{TA} = S_0^{TA} + G_{TA}^{TA} L_{TA}^{TA}$ lifting the foot segment into the neutral position (right angle with the shank). The parameter values for all gains and offsets are reported in table I.

C. Hip Control

We implement the hip portion of the modular control (1) by stimulating the hip extensor (gluteus group, GLU) and the hip flexor (HFL) (Fig. 3A), using the stretch feedback from RF for HFL and from HAM for GLU,

$$S^{\text{HFL}}(t) = S_0^{\text{HFL}} + G_{\text{RF}}^{\text{HFL}} L_{\text{RF}}^{\text{HFL}}(t - \Delta t_{\text{RF}}^{\text{HFL}}), \tag{11}$$

$$S^{\text{GLU}}(t) = S_0^{\text{GLU}} + G_{\text{HAM}}^{\text{GLU}} L_{\text{HAM}}^{\text{GLU}}(t - \Delta t_{\text{HAM}}^{\text{GLU}}). \tag{12}$$

We thus separate the flexion and extension part of the commanded torque in (1) observing that muscle can only pull in general and that HAM and RF in particular can go slack when the leg points backward and forward, respectively. Due to (9), the two stretch feedbacks jointly represent the first term in (1). We do not implement the second term with explicit neuromuscular control since the muscles' force-velocity relationship f_v automatically realizes a damping behavior. We detail how we realize the last, knee-hip-interaction term of (1) in the next section on knee control.

D. Knee Control

The neuromuscular interpretation of the knee control follows along with the three natural control tasks. We realize the first task by stimulating the short head of biceps femoris (BFsH), a monoarticular knee flexor, with a velocity feedback (10) from RF,

$$S^{\text{BFsH},i}(t) = G^{\text{BFsH}}_{\text{RF}} V^{\text{BFsH}}_{\text{RF}}(t - \Delta t^{\text{BFsH}}_{\text{RF}}), \qquad (13)$$

using $v^{\text{RF}}_{off} = 0$ (Fig. 3B). The zero offset automatically generates the velocity condition in (2) as the resulting muscle stimulation is bound to positive values.

For the second control task, we implement a length feedback L^{VAS} of the vasti (VAS), a group of monoarticular knee extensors. This feedback has no target muscle; it monitors leg length and engages the reflexes for the second task once the leg achieves sufficient ground clearance $l < l_{clr}$. (In humans, $l \propto \phi_k$ and $\phi_k - \phi_{k,i} = \mp 1/r^m_k (l^m_{ce} - l^m_{off})$ and $\dot{\phi}_k = \mp 1/r^m_k (v^m_{ce} - v^m_{off})$ for monoarticular knee extensors/flexors). During the second task, we realize the extension part (first line of Eq. 3) by stimulating RF with a velocity feedback from VAS

$$S^{\text{RF},ii}(t) = G^{\text{RF}}_{\text{VAS}} V^{\text{RF}}_{\text{VAS}}(t - \Delta t^{\text{RF}}_{\text{VAS}}). \qquad (14)$$

For the flexion part (second and third line), we stimulate BFsH with its own velocity feedback,

$$S^{\text{BFsH},ii}(t) = G^{\text{BFsH}}_{\text{BFsH}} V^{\text{BFsH}}_{\text{BFsH}}(t - \Delta t^{\text{BFsH}}_{\text{BFsH}})\, M, \qquad (15)$$

where M are modulating reflexes with $M = L^{\text{BFsH}}_{\text{RF}}(t - \Delta t^{\text{BFsH}}_{\text{RF}}) \cdot \left[V^{\text{BFsH}}_{\text{BFsH}}(t - \Delta t^{\text{BFsH}}_{\text{BFsH}}) + V^{\text{BFsH}}_{\text{RF}}(t - \Delta t^{\text{BFsH}}_{\text{RF}})\right]$. The first modulation reflex from the biarticular RF implements the term $(\alpha - \alpha_{tgt})$ of (3). The other modulation term in this equation, $(\dot{\phi}_k + \dot{\alpha})$, is implemented using the sum of two velocity reflexes from BFsH for $\dot{\phi}_k$ and from RF for $\dot{\alpha}$. These velocity reflexes also implicitly ensure the condition $\dot{\phi}_k > \dot{\alpha}$ for generating flexion torque.

The final control task of braking and extending the leg is implemented primarily by stimulating HAM and VAS (Fig. 3B). We use the biarticular stretch reflex

$$S^{\text{HAM},iii}(t) = G^{\text{HAM}}_{\text{HAM}} L^{\text{HAM}}_{\text{HAM}}(t - \Delta t^{\text{HAM}}_{\text{HAM}}) \qquad (16)$$

to stimulate HAM, which mimics the term $(\alpha_{thr} - \alpha)$ of (4) when using the offset value $l^{\text{HAM}}_{off} = -r^{\text{HAM}}_h(\alpha_{thr} - \alpha^{\text{HAM}}_r) - l^{\text{HAM}}_{sl} + l^{\text{HAM}}_0$. In addition, HAM proportionally recruits the synonymous knee flexors BFsH and GAS once its stimulation exceeds a threshold $S^{\text{HAM},iii} > S_{thr}$,

$$S^{\text{BFsH},iii}(t) = G^{\text{BFsH}}_{\text{HAM}} \left[S^{\text{HAM},iii}(t) - S_{thr}\right], \qquad (17)$$

$$S^{\text{GAS},iii}(t) = G^{\text{GAS}}_{\text{HAM}} \left[S^{\text{HAM},iii}(t) - S_{thr}\right], \qquad (18)$$

to prevent hyper extension of the knee caused by HAM torque saturation at high swing leg angular velocities. The second, velocity term of (4) is neglected in the control as the HAM's force-velocity relationship produces a similar damping behavior. However, we use a passive velocity feedback V^{HAM} to monitor when the leg angular velocity has slowed down to zero ($\dot{\alpha} = 0$), which triggers VAS stimulation by its own stretch reflex,

$$S^{\text{VAS},iii}(t) = G^{\text{VAS}}_{\text{VAS}} L^{\text{VAS}}_{\text{VAS}}(t - \Delta t^{\text{VAS}}_{\text{VAS}}), \qquad (19)$$

to extend the knee.

Although the muscle reflexes are introduced along with the three control tasks, they are active throughout swing without the separation into task-related phases. For instance, the total stimulation of BFsH is generated by $S^{\text{BFsH},tot} = S^{\text{BFsH},i} + S^{\text{BFsH},ii} + S^{\text{BFsH},iii}$. The only exceptions is the VAS extension reflex, which is connected only after $\dot{\alpha} = 0$ in the last task.

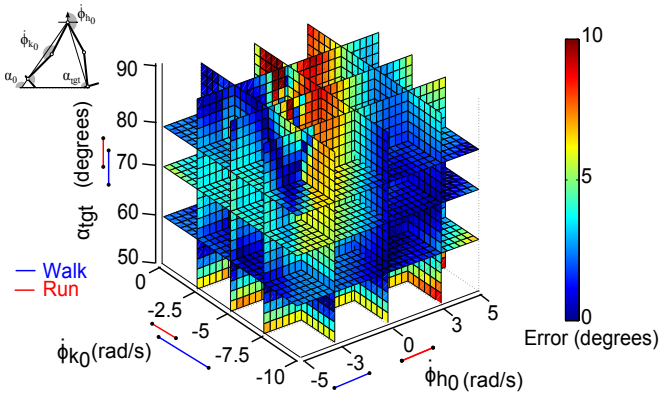

Fig. 4. Swing leg placement error for neuromuscular control model. The leg is hinged and the initial configuration is set to $\phi_{h,0} = 220$ deg, $\phi_{k,0} = 175$ deg ($\alpha_0 = 132.5$ deg), and $\phi_{a,0} = 120$ deg. The clearance leg length is set to $l_{clr} = 5cm$. See caption of figure 2 for additional explanations.

IV. Results

A. Leg placement into arbitrary targets

We tune the control parameters of the neuromuscular model by hand with two goals in mind. First, with the application to autonomous prostheses in mind, we seek a single set of parameters that minimizes the error between the landing leg angle and its target α_{tgt} for a large range of initial joint velocities and target angles exceeding those of human walking and running. Second, we require the corresponding joint torques to stay within experimentally observed ranges.

The identified set of control parameters is shown in table I. Except for α_{thr}, which differs between walking and running (12/24 deg respectively), parameters remain constant. The larger threshold angle for activating HAM earlier in running than in walking is needed to prevent knee hyper-extension. Such an earlier activation is also observed in humans [22].

The achieved performance of target placement with the neuromuscular system is shown in Fig. 4. For target angles α_{tgt}= 50...75 deg and for initial joint velocities $\dot{\phi}_{h,0} = -5 \ldots 5$ rads^{-1} and $\dot{\phi}_{k,0} = -10 \ldots 0$ rads^{-1}, the average and maximum placement errors are 2.8 deg and 9.2 deg. These errors compare with the performance of the ideal control (Sec. II) and cover typical human landing leg angles and initial joint speeds observed in walking and running. For steeper target angles, however, the placement shows clearly larger error due to the toe dragging the ground.

TABLE I

CONTROL PARAMETER VALUES. OTHER PARAMETERS ARE ADAPTED FROM [19]

Gains				Offsets	
$G^{\text{TA}}_{\text{TA}}$	25	$G^{\text{BFsH}}_{\text{BFsH}}$	1.25	l^{RF}_{off}	0.059 (m)
$G^{\text{HFL}}_{\text{RF}}$	0.5	$G^{\text{HAM}}_{\text{HAM}}$	2	l^{HAM}_{off}	0.0716 (m)
$G^{\text{GLU}}_{\text{HAM}}$	0.5	$G^{\text{BFsH}}_{\text{HAM}}$	3	l^{VAS}_{off}	0.0324 (m)
$G^{\text{BFsH}}_{\text{RF}}$	0.1	$G^{\text{GAS}}_{\text{HAM}}$	2	l^{TA}_{off}	0.0432 (m)
$G^{\text{RF}}_{\text{VAS}}$	0.14	$G^{\text{VAS}}_{\text{VAS}}$	0.05	S_{thr}	0.65

B. Comparison to human walking and running

To compare the resulting swing leg motions to actual human leg motions, we recorded swing leg trajectories of a subject walking at slow to fast speeds (0.65ms^{-1} to 2ms^{-1}) and running at slow to moderately fast speeds (2.5ms^{-1} to 5.5ms^{-1}). The subject's ankle trajectories and corresponding hip and knee torques during swing are shown in the left column of figure 5. The right column shows the patterns predicted by the neuromuscular model. (Note that for the comparison we applied the observed hip translational accelerations and leg initial conditions to the model.) In addition, figure 6 compares the time history of muscle activations generally observed in walking and running (adapted from [23]) with those predicted by the model for matched speeds.

In walking, the swing leg patterns predicted by the model are similar to the ones observed in humans. The ankle trajectories have a similar range and shape in particular for slower walking speeds (Fig. 5A), and the hip and knee torques have similar magnitudes and gross behavior except for the larger initial torques in human walking at 2ms^{-1} (Fig. 5B,C). The activation patterns for the hip muscles HFL and GLU show similar timings and magnitudes between the model and humans (Fig. 6A). Although the knee muscle activation patterns show a similar trend (Fig. 6B), some deviations occur with respect to the onset time for BFsH, which is delayed. For the ankle muscles, TA misses the late swing activation seen in humans in preparation for stance (Fig. 6C), a known shortcoming of the ankle control we took from [19].

In contrast to walking, the patterns for running show more deviations between the model and humans. The model has a shorter stride length and a clearly faster swing time than present in human running (Fig. 5D). Despite these differences, the shapes of the torque patterns match human data in general (5E,F). In the activation patterns, humans have an increased tonus for all muscles that is absent in the model (Fig. 6). In addition to this muscle tonus, the activities of BFsH and GAS show different characteristic features. In humans, BFsH has a prominent activation peak that coincides with RF peak activation (Fig. 6B). By contrast, in the model, the early BFsH peak occurs at the very beginning of swing and RF activity onset is delayed. Further, the model shows an activation burst of GAS at the end of swing due to the synonymous activation (18) that humans do not seem to have to such an extent (Fig. 6C).

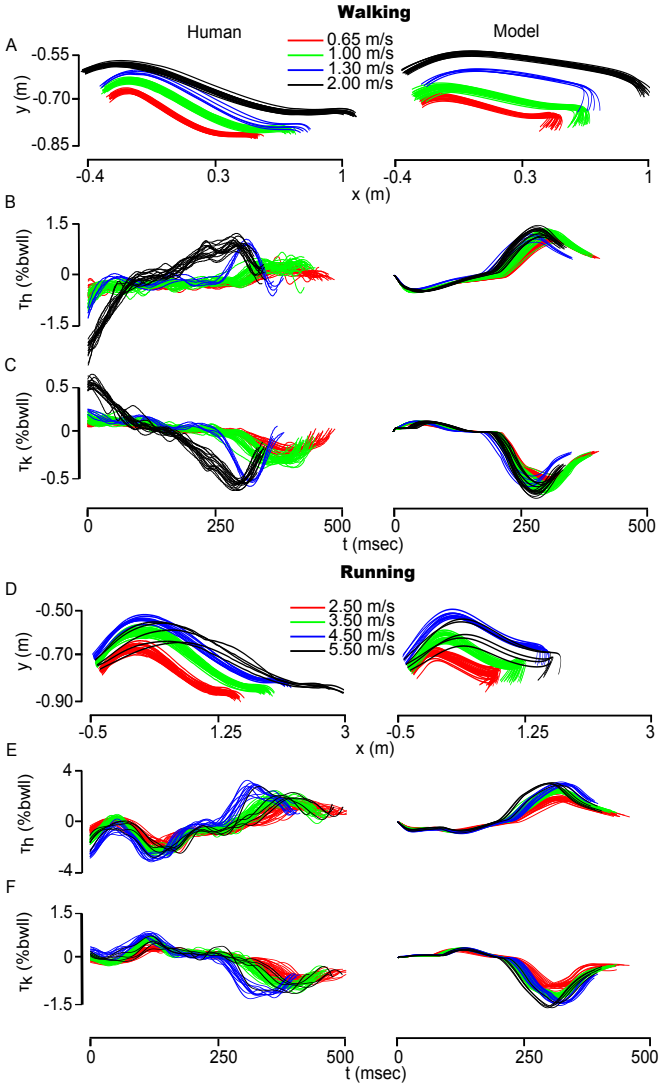

Fig. 5. Observed and predicted swing leg patterns in walking and running. The ankle trajectories (**A**,**D**), hip and knee torques (**B**,**C**,**E**,**F**) of multiple swing phases (individual traces) are compared between human and model at different speeds (color coded). For the model, the initial joint positions and speeds as well as the hip translational accelerations are taken from the corresponding human swing motions. The target angle is set to the observed (average) landing angle $\alpha_{tgt} = 70$ deg. The ankle trajectories are given with respect to a world frame that originates at the initial position of the hip. The torques are normalized to percent of body weight times leg length (%bwll).

V. CONCLUSION AND FUTURE WORK

In previous work, we identified a control for a double pendulum leg in swing that is based on local feedbacks and does not require predefined trajectories to robustly place the leg into target points on the ground in the presence of large disturbances [17]. To compare the identified control with human swing leg behavior at the level of muscle activations, and to prepare a transfer to powered prosthetic legs that can react like human limbs, we here developed a neuromuscular model of the human leg in swing and interpreted the identified control with local muscle reflexes.

The resulting reflex control robustly places the swing leg

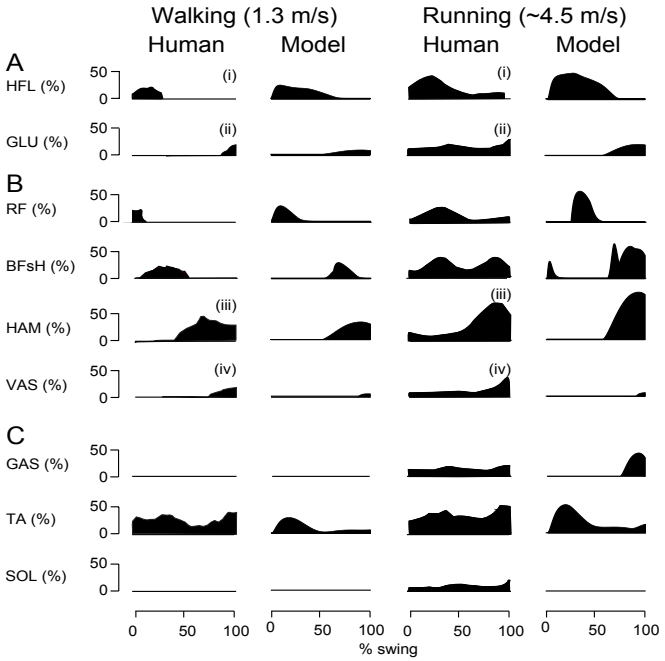

Fig. 6. Observed and predicted muscle activations in walking and running. Steady-state patterns of muscle activations during swing are shown for hip (**A**), knee (**B**) and ankle muscles (**C**). Human data adapted from [23]. Compared muscles: (i) iliacus (ii) upper gluteus maximum, (iii) semimembranosis, and (iv) vastus lateralis.

into target angles from 50 deg to 75 deg which cover observed landing leg angles for a wide range of human walking and running speeds (Fig. 4). In addition, the control generates swing patterns that share the main features of human swing leg patterns for the ankle trajectory, joint torques, and muscle activations (Figs. 5 and 6). Main differences occur in running where the neuromuscular model produces shorter strides and stride times than humans and where the model's muscle activation patterns cannot capture some characteristic features in timing and amplitude of GLU, BFsH, VAS and TA as well as the overall increase in muscle tonus. In part, these differences can be avoided by changing control parameters between walking and running. For instance, changing the clearance length l_{clr} will influence the placement accuracy for steep landing angles, the initial joint torques, and the timing of the muscle patterns during early swing.

In the future, we plan to use the comparison between the neuromuscular control model and EMG measurements in humans to extract ideas about how to refine and improve the autonomous swing leg control for robotic applications. This direction will also include the integration of the developed swing control into an existing neuromuscular model of human walking [19] to study the response to disturbances like tripping and slipping. In addition, we plan to transfer the autonomous swing control to robotic legs in humanoid and rehabilitation robotics, for which we are currently developing a robotic leg testbed [24].

REFERENCES

[1] M. Raibert, *Legged robots that balance*. MIT press, Cambridge, 1986.

[2] J. Hodgins and M. N. Raibert, "Adjusting step length for rough terrain locomotion," *IEEE Trans on Robotics and Automation*, vol. 7, no. 3, pp. 289–298, 1991.

[3] S. Kajita, F. Kanehiro, K. Kaneko, K. Yokoi, and H. Hirukawa, "The 3d linear inverted pendulum mode: a simple modeling for a biped walking pattern generation," in *IEEE/RSJ International Conference on Intelligent Robots and Systems*, vol. 1, 2001, pp. 239 –246 vol.1.

[4] J. Pratt, J. Carff, S. Drakunov, and A. Goswami, "Capture point: A step toward humanoid push recovery," in *Proceedings of the 6th IEEE-rAS Intl Conf on Humanoid Robots*, 2006.

[5] F. Parietti and H. Geyer, "Reactive balance control in walking based on a bipedal linear inverted pendulum model," in *IEEE Int Conf on Robotics and Automation*, 2011, pp. 5442–5447.

[6] A. Wu and H. Geyer, "The 3d spring-mass model reveals a time-based deadbeat control for highly robust running and steering in uncertain environments," *IEEE Trans on Robotics*, submitted.

[7] J. Morimoto, G. Zeglin, and C. G. Atkeson, "Minimax differential dynamic programming: Application to a biped walking robot," in *IEEE/RSJ Int. Conf. on Intelligent Robots and Systems*, 2003, pp. 1927–1932.

[8] P. Michel, J. Chestnutt, S. Kagami, N. Koichi, J. Kuffner, and T. Kanade, "Gpu-accelerated real-time 3d tracking for humanoid locomotion and stair climbing," in *IEEE/RSJ Int. Conf. on Intelligent Robots and Systems*, 2007, pp. 463–469.

[9] M. Kanako, M. Mitsuharu, F. Kanehiro, S. Kajita, K. Kaneko, and K. Yokoi, "Human-like walking with toe supporting for humanoids," in *IEEE/RSJ Int. Conf. on Intelligent Robots and Systems*, 2011, pp. 4428–4435.

[10] J. L. Johansson, D. M. Sherrill, P. O. Riley, P. Bonato, and H. Herr, "A clinical comparison of variable-damping and mechanically passive prosthetic knee devices," *American Journal of Physical Medicine and Rehabilitation*, vol. 84, no. 8, pp. 563–575, 2005.

[11] S. K. Au, H. Herr, J. Weber, and E. C. Martinez-Villalpando, "Powered ankle-foot prosthesis for the improvement of amputee ambulation," *Conf Proc IEEE Eng Med Biol Soc*, vol. 2007, pp. 3020–6, 2007.

[12] K. Fite, J. Mitchell, F. Sup, and M. Goldfarb, "Design and control of an electrically powered knee prosthesis," in *Proc IEEE Int Conf on Rehabilitation Robotics*, 2007, pp. 902–905.

[13] M. Holgate, A. Bohler, and T. Sugar, "Control algorithms for ankle robots: A reflection on the state-of-the-art and presentation of two novel algorithms," in *2nd IEEE RAS EMBS International Conference on Biomedical Robotics and Biomechatronics*, 2008, pp. 97 –102.

[14] M. L. Shik, F. V. Severin, and G. N. Orlovski, "Control of walking and running by means of electric stimulation of the midbrain," *Biofizika*, vol. 11, no. 4, pp. 659–666, 1966.

[15] G. Courtine, Y. Gerasimenko, R. van den Brand, A. Yew, P. Musienko, H. Zhong, B. Song, Y. Ao, R. M. Ichiyama, I. Lavrov, R. R. Roy, M. V. Sofroniew, and V. R. Edgerton, "Transformation of nonfunctional spinal circuits into functional states after the loss of brain input," *Nat Neurosci*, vol. 12, no. 10, pp. 1333–42, 2009.

[16] H. Hultborn and J. B. Nielsen, "Spinal control of locomotion - from cat to man," *Acta Physiologica*, vol. 189, no. 2, pp. 111–121, 2007.

[17] R. Desai and H. Geyer, "Robust swing leg placement under large disturbances," in *IEEE Int Conf on Robotics and Biomimetics*, submitted.

[18] K. Hunt and F. Crossley, "Coefficient of restitution interpreted as damping in vibroimpact," *Journal of Applied Mechanics*, vol. 42, no. 2, pp. 440–445, 1975.

[19] H. Geyer and H. Herr, "A muscle-reflex model that encodes principles of legged mechanics produces human walking dynamics and muscle activities," *IEEE Trans Neural Syst Rehabil Eng*, p. DOI 10.1109/TNSRE.2010.2047592, 2010.

[20] D. A. Winter, *Biomechanics and motor control of human movement*, 4th ed. Hoboken, N.J.: Wiley, 2009.

[21] H. Hultborn, "Spinal reflexes, mechanisms and concepts: from Eccles to Lundberg and beyond." *Prog Neurobiol*, vol. 78, no. 3-5, pp. 215–232, 2006.

[22] M. G. J. Gazendam and A. L. Hof, "Averaged emg profiles in jogging and running at different speeds," *Gait Posture*, vol. 25, no. 4, pp. 604–14, 2007.

[23] J. Perry, *Gait analysis: normal and pathological function*. SLACK Inc., Thorofare, NJ, 1992.

[24] A. Schepelmann, M. Taylor, and H. Geyer, "Development of a testbed for robotic neuromuscular controllers," in *Proceedings of Robotics: Science and Systems*, 2012.